ACS OMEGA

http://pubs.acs.org/journal/acsodf

Article

Synthesis of MoS_2 Nanochains by Electrospinning for Ammonia Detection at Room Temperature

Aoqun Jian,[†] Junhe Wang,[†] Hongying Lin, Shiqiang Xu, Dan Han, Zhongyun Yuan, and Kai Zhuo*

Cite This: *ACS Omega* 2022, 7, 11664−11670

Read Online

ACCESS | Metrics & More | Article Recommendations

ABSTRACT: MoS_2 nanochains were successfully prepared via facile electrospinning and a hydrothermal process. The morphology of MoS_2 nanochains was evaluated by field emission scanning electron microscopy and high-resolution transmission electron microscopy. A slurry composed of the MoS_2 nanochains was coated on a silver electrode to detect ammonia. The detection range of ammonia was between 25 and 500 ppm. MoS_2 nanochains offered outstanding sensing response, repeatable reproducibility, and excellent selectivity with a detection limit of 720 ppb. The responsiveness of MoS_2 nanochains to ammonia remained unchanged for 1 week.

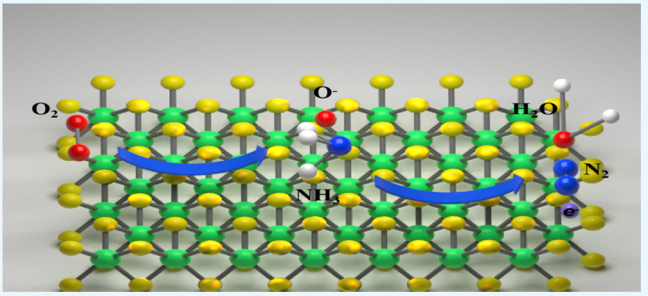

1. INTRODUCTION

Ammonia (NH_3) is an air pollutant released during agriculture, livestock, and industrial combustion processes.[1] At higher concentrations, it can damage human organs, thus leading to a range of inflammatory conditions such as headaches, breathing difficulties, and even death. Damage can also occur when humans are exposed to low concentrations for extended periods of time.[2] Thus, it is crucial to develop a ppm-level ammonia sensor monitor.

A variety of sensing techniques are available for ammonia detection; the most prevalent detection methods can be divided into three main categories, namely, solid-state sensing methods (metal oxide-based sensors and conductive polymer sensors), optical methods (optical sensors using tunable diode laser spectroscopy), and other methods (electrochemical sensors, surface acoustic wave sensors, and field effect transistor sensors).[3] To date, various gas sensing materials have been reported to detect ammonia, including metal oxides, conducting polymers, and transition metal disulfides (TMDs).[4−6] However, metal oxides are mostly used for conventional rigid chemical gas sensors and require high operating temperatures, consume high levels of power, and have safety hazards. Metal oxides also have low selectivity in detecting a specific gas from a gas mixture.[7]

Conducting polymers can significantly improve sensing performance when used as ammonia-sensitive materials. However, conducting polymers have intrinsic shortcomings such as sluggish reaction kinetics, poor mechanical strength, and insufficient stability. Thus, to address the shortcomings of these materials, attention has shifted to TMDs.

TMDs have been widely used in sensors, photocatalysis, and supercapacitors. Molybdenum disulfide (MoS_2) has received increasing attention due to its large direct band gap (1.2−1.9 eV), high surface area-to-volume ratio, and excellent field effect transistor (FET) behavior. As an important n-type semiconductor, the two-dimensional (2D) layered structures of MoS_2 are a promising gas sensing material due to their large surface area-to-volume ratio, high carrier mobility, and various active sites, e.g., sulfur defects, vacancies, and edge sites.[8] Previous studies have shown that active sites on 2D MoS_2 for gas sensors mainly derive from sulfur edges rather than basal planes.[9] Thus, many strategies have been devoted to increasing the density of sulfur edge sites for the enhancement of MoS_2 gas sensor performance including vertically grown MoS_2 layers,[10] nanoflowers,[11] and quantum dots.[12] In particular, some new excitement in MoS_2 has been sparked by emerging single or thin-layered 2D MoS_2 structures because the thickness of MoS_2 nanosheets was highly related to the surface-to-volume ratio and semiconducting properties—in turn, these affect sensitivity.[13] Moreover, the terminating sulfide at the edges of MoS_2 could have maximum exposure in the case of thin-layered MoS_2.[1414] Most of the early studies used mechanical stripping or sputtering deposition to prepare molybdenum disulfide, and the resulting molybdenum disulfide was in the form of layers.[15] Later, chemical vapor deposition was used to prepare molybdenum disulfide films;[16] nanoflower

Received: November 16, 2021
Accepted: January 27, 2022
Published: March 29, 2022

ACS Publications

© 2022 The Authors. Published by American Chemical Society

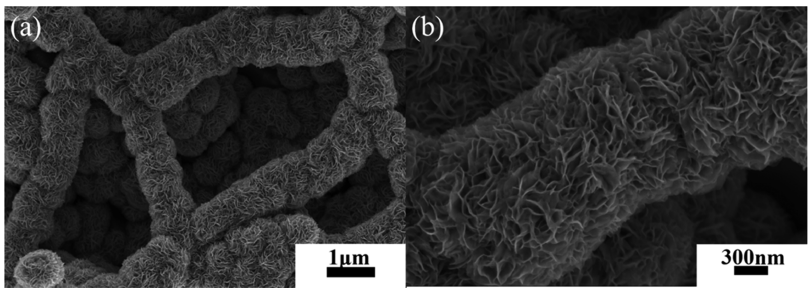

Figure 1. Low-magnification (a) and high-magnification (b) SEM images of MoS_2 nanochains.

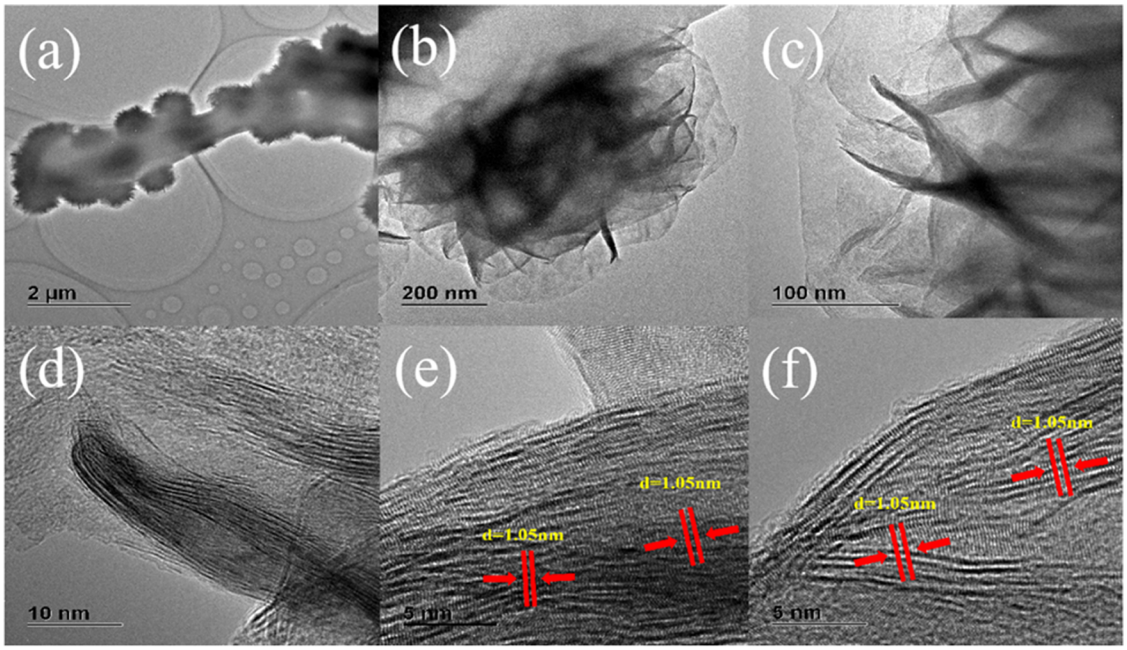

Figure 2. TEM (a–d) and HRTEM (e, f) images of MoS_2 nanochains.

molybdenum disulfide has also been prepared using a hydrothermal process.[11] Electrospinning as a nanomaterial preparation method features a long length of the output nanofiber, uniform scale, and the ability to control the fiber diameter.

In this work, MoS_2 nanochains were synthesized by electrospinning and a hydrothermal process. The morphologies, nanostructures, and compositions of MoS_2 nanochains were obtained from field emission scanning electron microscopy, transmission electron microscopy, X-ray diffraction, Raman spectroscopy, and X-ray photoelectron spectroscopy. The MoS_2 nanochains were used to detect different concentrations of ammonia with good reproducibility, selectivity, and stability

2. EXPERIMENTAL PROCEDURE

2.1. Reagent and Instruments. Sodium molybdate dihydrate ($Na_2MoO_4{\cdot}2H_2O$, ≥99.95%), thiourea (CH_4N_2S, ≥99.95%), *N*,*N*-dimethylformamide (DMF, 99.9%), polyacrylonitrile (PAN, M_w = 150 000), and graphene oxide (GO, >99%) were purchased from China National Pharmaceutical Group.

Electrospinning equipment (YFSP-T, Tianjin Yunfan) was used to prepare and synthesize nanofiber materials. The morphology of MoS_2 nanochains was characterized using field emission scanning electron microscopy (FE-SEM, ZEISS Gemini SEM300), transmission electron microscopy (TEM, JEM-2100F03040702), X-ray diffraction (XRD, SHIMADZU XRD-6100), Raman spectra (Renishaw Qontor), and X-ray photoelectron spectroscopy (XPS, ThermoFisher Thermo). A Sino Aggtech, IST500E was used to detect ammonia.

2.2. Synthesis of Samples. GO (15 mg) was dispersed into 18 mL of DMF through sonication for 30 min. The GO dispersion contained 1.8 g of PAN and was stirred in a water bath at 80 °C for 4 h. The solution was then transferred into a 5 mL syringe for electrospinning. The complex nanofibers were generated with an electrospinning voltage of 18 kV and an injection rate of 2.25×10^{-3} mL/min. The complex nanofibers were heated at 280 °C for 2 h at a heating rate of 5 °C/min.

Next, $Na_2MoO_4{\cdot}2H_2O$ (0.242 g) and 0.305 g of $CS(NH_2)_2$ were dissolved into 60 mL of deionized water and stirred for 30 min; 2.7 g of complex nanofibers were dispersed into 30 mL of the above solution by sonication for 10 min and then transferred into a 50 mL Teflon-lined stainless steel autoclave. The stainless steel autoclave was maintained at 210 °C for 24 h. The process was repeated several times by centrifugation at 4000 rpm for 10 min. The precipitate was washed with deionized water to obtain MoS_2 nanochains.

2.3. Preparation of MoS_2 Nanochain Electrodes and Gas Sensing Measurements. The resulting MoS_2 nanochains were ground in a mortar and then deionized water was added to make a paste. This paste was then applied to a quartz

https://doi.org/10.1021/acsomega.1c06456
ACS Omega 2022, 7, 11664–11670

substrate with predeposited silver electrodes spaced at 5 mm intervals. After applying a thick paste, the resulting device was dried in a vacuum oven at 60 °C for 2 h. These devices were used for electrical and sensing measurements.

The gas sensing characteristics were measured under static conditions at room temperature (25 ± 2 °C, 15 ± 2% RH). Ammonia gas samples were prepared as follows. Ammonia at 25−500 ppm was obtained by evaporating ammonia (aq) from the heater in the test chamber. The gas response was defined as $S = \frac{R_a - R_g}{R_a} \times 100\%$, where R_a and R_g are the resistances of the gas sensor in air and test gas, respectively. Response time and recovery time were calculated from the time required for adsorption and desorption conditions.

3. RESULTS AND DISCUSSION

3.1. Characterization Results. Figure 1a shows a representative morphology of the complex nanofibers modified with three-dimensional hydrangea-like MoS_2 nanospheres. The dense MoS_2 nanospheres were uniformly modified on the complex nanofibers with a new morphology and a peculiar nanochain structure. The high-magnification SEM images in Figure 1b show that the MoS_2 nanospheres consisted of MoS_2 nanoplates that were uniformly distributed and cross-aligned; MoS_2 nanochains with a diameter of about 1 μm can also be observed. The unique nanochain structure ensured a high specific surface area, resulting in better adsorption and desorption processes for gas detection.

Figure 2a shows three-dimensional hydrangea-like MoS_2 nanospheres: These were tightly and uniformly immobilized on the surface of the complex nanofibers. Figure 2b shows a single MoS_2 nanosphere; the MoS_2 nanosphere was formed by interlocking stacks of MoS_2 nanoplates. Figure 2c,d shows a monolayer MoS_2 nanoplate dispersed in carbon. The HRTEM images (Figure 2e,f) suggest that the interlayer distance between the MoS_2 nanoplates was 1.05 nm. This was due to the expansion of two adjacent MoS_2 layers because of the addition of carbon; this is discussed in the XRD section below.

The XRD patterns of the MoS_2 nanochains are shown in Figure 3. The pattern for MoS_2 nanochains was compared with

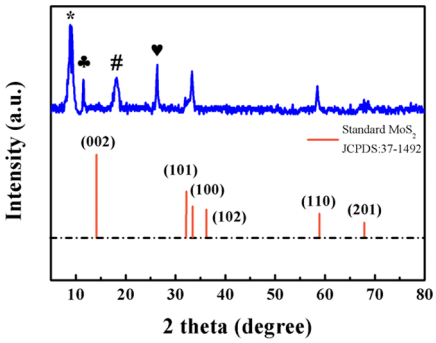

Figure 3. XRD pattern of the prepared MoS_2 nanochains.

a hexagonal structure (JCPDS 37-1492). Figure 3 shows that the peaks of (002), (101), and (102) were not found in the prepared samples. Only three peaks of MoS_2 nanochains—(100), (110), and (201) peaks—were observed. A weak diffraction peak was found at 2θ = 25.1° (see Figure 3, marked by the heart symbol); these peaks were attributed to the (002) plane of carbon. The absence of the (002) reflection of MoS_2 suggested no monolayer stacking—this implied that MoS_2 in the composite should have a single-layer structure, which was confirmed by HRTEM. In addition, there were three new diffraction peaks of MoS_2 nanochains near 2θ = 9, 11.5, and 18° (Figure 3); these are marked by the #, clubs, and * symbols. The diffraction peak marked by the clubs symbol was the characteristic peak of graphene oxide. The other two peaks (# and *) were indexed to neither MoS_2 nor carbon. These two peaks might be due to the intercalation of MoS_2 and carbon. The *d*-spacing corresponding to the two peaks (* and #) was calculated according to the diffraction angles using the Bragg equation: 1.01 (*) and 0.49 (#) nm. It is well-known that the *d* (002)-spacing values of MoS_2 and carbon are 0.61 and 0.34 nm, respectively. The *d*-spacing of peak * was 0.49 nm, which was between the *d* (002) of MoS_2 and carbon. Peak # might represent the spacing of MoS_2 and carbon. The *d*-spacing of peak # was 1.01 nm, which was twice the *d*-spacing of peak *; this might be the distance of neighboring MoS_2. This conclusion has been verified by Chang et al.[17]

Figure 4a shows the Raman spectra of the prepared MoS_2 nanochains. Two characteristic peaks were observed at 398.8 and 374.4 cm^{-1} associated with the A_{1g} mode due to the out-of-plane vibrations of sulfur atoms; the E_{2g} mode relates to the in-plane vibrations of Mo and S atoms, respectively. The distance between the two characteristic peaks was related to the number of MoS_2 layers. The distance was 24.4 cm^{-1} and could be observed in Figure 4a, which indicated that MoS_2 was a single layer. Figure 4b shows the Raman spectrum of GO as a part of the MoS_2 nanochains.

Figure 5a−d indicates the XPS spectra of MoS_2 nanochains, Mo 3d, S 2P, and O 1s. Figure 5a shows the entire measured spectrum, confirming the presence of Mo, S, C, and O in the composite. The spectrum of Mo 3d (Figure 5b) shows two peaks located at 228.48 and 232.68 eV corresponding to Mo $3d_{5/2}$ and Mo $3d_{3/2}$, respectively, which is likely the Mo^{4+} of MoS_2.[18] There was a peak of lower binding energy at 226.08 eV, which is consistent with S^{2-} 2s.[19] Moreover, two minor peaks at 235.98 and 232.98 eV were characteristic peaks of Mo^{6+} $3d_{3/2}$ and Mo^{6+} $3d_{5/2}$, respectively, for Mo−O bonds, suggesting the introduction of oxygen on the MoS_2 surface.[13] Figure 5c further shows the XPS spectra of S 2p where the peaks at 162.98 and 161.68 eV were attributed to S $2p_{1/2}$ and S $2p_{3/2}$, respectively.[20,21] The C 1s region (Figure 5d) has two peaks at 286.68 and 284.78 eV matching C−C and C−O, respectively. These data confirmed the presence of MoS_2, C, and GO.

3.2. Gas Sensor Characteristics. To evaluate the advantages of MoS_2 nanochains, the as-prepared products were evaluated as sensing materials for ammonia at room temperature (RT). The sensor was studied at different concentrations of ammonia. Figure 6a shows the response characteristics of the MoS_2 nanochains for ammonia from 25 to 500 ppm at room temperature. The response of MoS_2 nanochains increased with increasing ammonia concentration. The MoS_2 nanochains had a high ammonia gas sensing response above 71% at 500 ppm ammonia. This high sensitivity was due to the nanochain structure and high surface area.

Reproducibility is a major issue in gas sensing. Five response−recovery tests were repeated for 200 ppm ammonia at room temperature to evaluate reproducibility. All of the responses were essentially stable at the same level (40%), suggesting that the MoS_2 nanochains were repeatable for ammonia detection (Figure 6b).

https://doi.org/10.1021/acsomega.1c06456
ACS Omega 2022, 7, 11664−11670

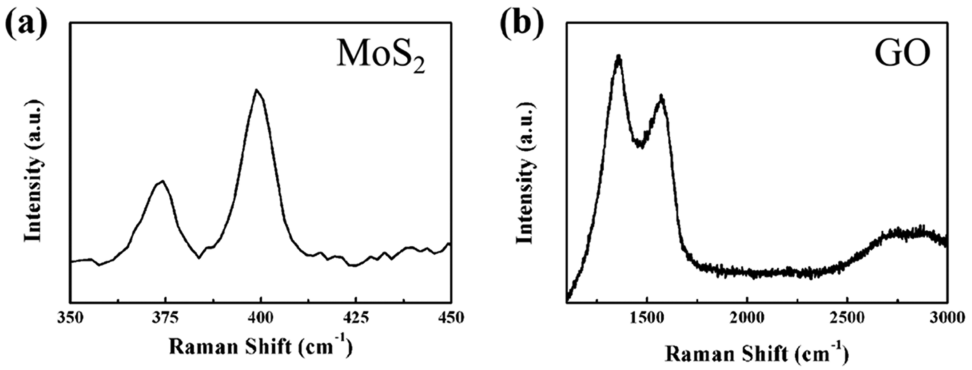

Figure 4. Raman spectra of MoS_2 (a) and GO (b).

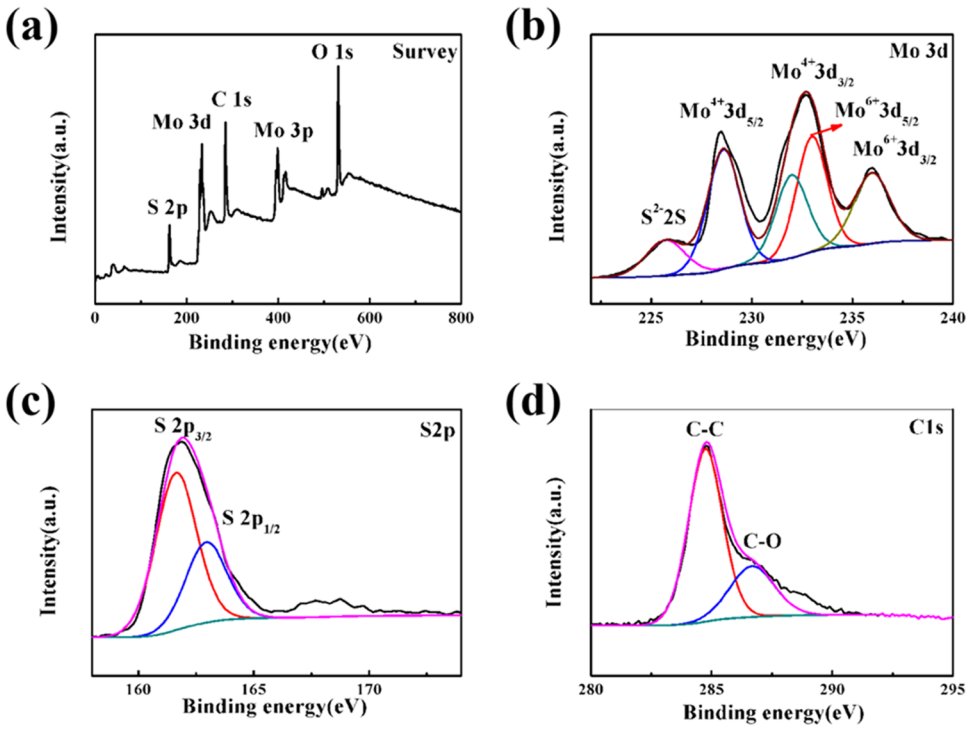

Figure 5. XPS survey spectra of MoS_2 nanochains (a). High-resolution XPS spectra of Mo 3d (b), S 2p (c), and C 1s (d).

Selectivity is also a significant indicator of gas sensors. Therefore, the MoS_2 nanochains were tested against 200 ppm ammonia, acetone, ethanol, isopropanol, nitrogen dioxide, and formaldehyde (Figure 6c). The results indicate that the MoS_2 nanochains had excellent selectivity for ammonia. Long-term stability experiments were conducted by exposing MoS_2 nanochains to ammonia at 200 ppm for several consecutive days, and the test results are shown in Figure 6d. The response of the MoS_2 nanochains remained constant for one week, but they subsequently decreased by about 10%.

Humidity has a large impact on the gas sensor, and we have tested the sensor for different humidity levels (200 ppm ammonia, room temperature), and the results are shown in Figure 7. As shown in Figure 8, the response of the sensor hardly changes as the humidity increases, but we find that the response/desorption time gradually becomes longer as the humidity increases.

Figure 8a shows a linear function response of the MoS_2 nanochains to the ammonia concentration. The fitted relationship for MoS_2 nanochains is $Y = 0.73291 + 0.00434x$. The MoS_2 nanochains had a higher linear coefficient. According to the International Union of Pure and Applied Chemistry (IUPAC), the detection limit of a sensor is generally defined as three times the standard deviation of its noise.[22] The noise of the sensor can be calculated using the relative resistance variation of the base resistance using the root-mean-square deviation. Here, 10 data points were taken on the MoS_2 nanochain electrode prior to exposure to ammonia (Figure 8b). After plotting the data, a fifth-order polynomial fit was performed over the range of data points. This was done not only for curve fitting but also for statistical parameters of the polynomial fit. The noise was calculated as

$$N = \sqrt{\frac{\sum (S_i - S)^2}{T}}$$

Here, S_i is the measured data point, S is the corresponding value calculated from the curve fitting equation, and T is the number of data points used in the curve fitting. According to the IUPAC definition, the signal is considered to be real when the signal-to-noise ratio equals 3.[23] Therefore, the theoretical

https://doi.org/10.1021/acsomega.1c06456
ACS Omega 2022, 7, 11664−11670

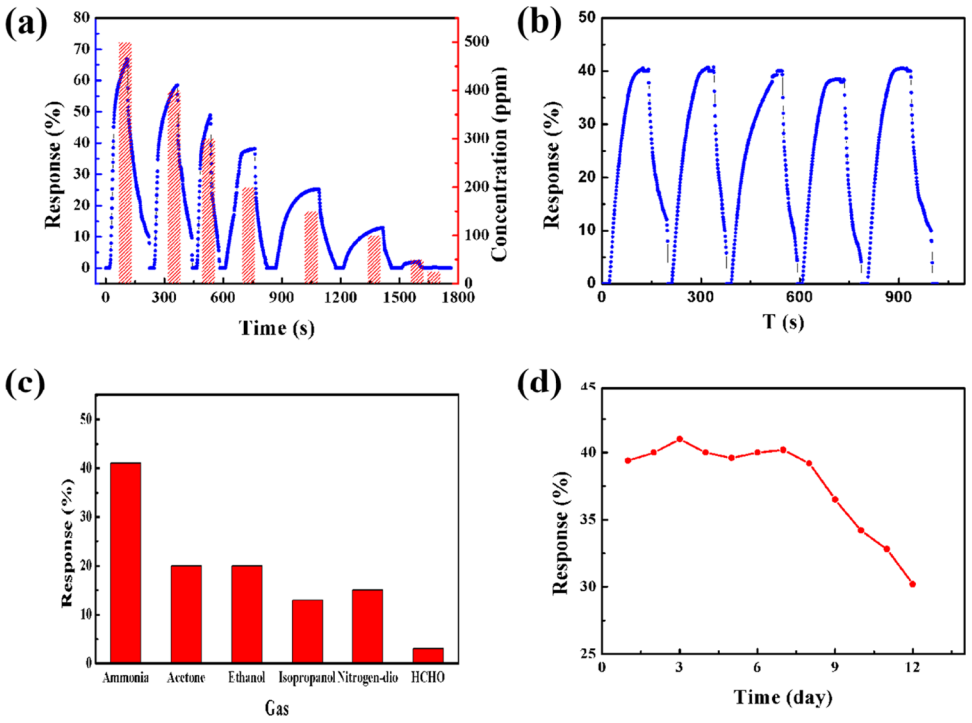

Figure 6. Detection of 25−500 ppm ammonia at room temperature (a), 200 ppm ammonia reproducibility (b), selective detection of five kinds of gases (c), and the long-term stability of 200 ppm ammonia detection (d).

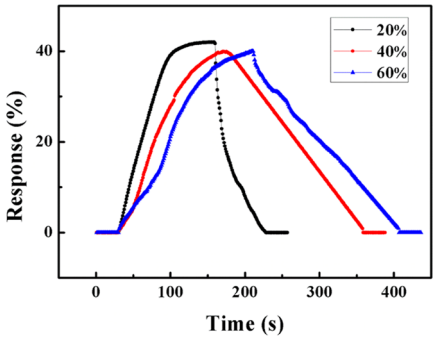

Figure 7. Response curves obtained from the detection of 200 ppm ammonia in different humidity environments.

detection limit (DL) was calculated using the following equation

$$\mathrm{DL} = 3\frac{N}{\mathrm{slope}}$$

Here, slope is extrapolated from the linear function of ammonia concentration as shown in Figure 8a. The DL of MoS_2 nanochains was 720 ppb. This suggested potential applications in environmental monitoring and breath analysis.

Table 1 compares the gas sensing performance between MoS_2 nanochains and other materials for ammonia detection. The comparison results showed that MoS_2 nanochains have superior or comparable ammonia sensing performance to other materials. This indicates that the MoS_2 nanochains were conducive to ppm-level ammonia detection.

3.3. Sensing Mechanism. The resistance of the MoS_2 nanochains in contact with ammonia varies with time and can probe the mechanism of MoS_2 nanochains' sensitivity to gas (Figure 9). When the MoS_2 nanochains were exposed to ammonia, the resistance decreases to a minimum value depending on the level of ammonia. The resistance returns

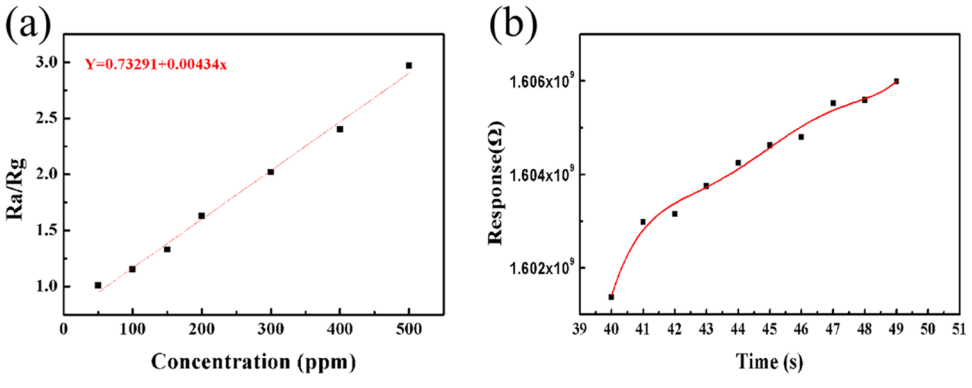

Figure 8. Response curves of the sensor to different concentrations were fitted (a), and 10 points were obtained under normal conditions (b).

https://doi.org/10.1021/acsomega.1c06456
ACS Omega 2022, 7, 11664−11670

Table 1. Comparison of the Sensing Performance of the Sensor in This Work with Other Previously Reported Ammonia Sensors

materials	temp. (°C)	DL	response	ref
MoS_2/graphene	RT	720 ppb	40% (200 ppm)	this work
MoS_2/Au	60 °C		10 (1000 ppm)	24
MoS_2/WO_3	200 °C	25 ppm	70% (200 ppm)	25
MoS_2/SnO_2	RT	50 ppm	10 (50 ppm)	26
SnO_2/MoS_2	50 °C	1 ppm	6.51 (10 ppm)	27
MXene	RT	500 ppb	6% (500 ppm)	28
PANI/SnO_2	RT	10 ppm	30% (100 ppm)	29

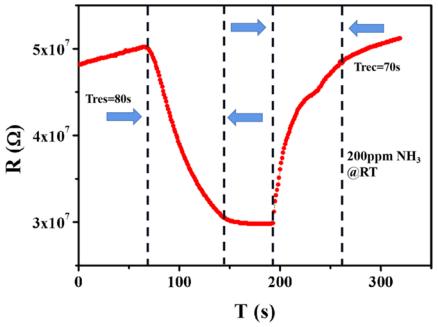

Figure 9. Resistance change curve of the MoS_2 sensor for 200 ppm ammonia detection at room temperature.

to its baseline value when ammonia is removed from the chamber. Ammonia is a reducing gas, and thus the decrease in sensor resistance indicated that the MoS_2 nanochains behave like an n-type semiconductor.

Therefore, most of the electrons in n-type-semiconductor MoS_2 nanochains are carriers. In air, many oxygen molecules capture free electrons from the surface of MoS_2 materials and form O_2^-[9] as shown in the following reactions

$$O_2(gas) \rightarrow O_2(ads) \quad (1)$$

$$O_2(ads) + e^- \rightarrow O_2^-(ads) \quad (2)$$

$$O_2^-(ads) + e^- \rightarrow 2O^-(ads) \quad (3)$$

When ammonia is adsorbed on the surface, it reacts with the oxygen species and donates electrons to MoS_2[30] according to the following reaction

$$2NH_3 + 3O^- \rightarrow N_2 + 3H_2O + 3e^- \quad (4)$$

The process is shown in Figure 10. The electron transferred back to the surface of MoS_2 changes the surface resistance. Thus, the reaction mechanism depends entirely on the availability of oxygen and its reaction with ammonia molecules.

4. CONCLUSIONS

In summary, a new and simple fabrication method of MoS_2 nanochains was used in this study via electrospinning and a hydrothermal process. Structural analysis revealed that MoS_2 nanoplates were uniformly interlaced to form MoS_2 nanospheres, which in turn form the final nanochain structure on the electrospinning nanofibers. The change in the resistance of MoS_2 nanochains when performing ammonia detection proved that they are n-type semiconductors. Gas sensing measurement results indicated that MoS_2 nanochains exhibited a response of 40% toward 200 ppm ammonia, relatively rapid response and recovery times, good repeatability, excellent selectivity, stability in 1 week to ammonia at room temperature, and a detection limit of 720 ppb. Compared with other MoS_2-based materials, MoS_2 nanochains have better response and recovery properties and higher responsivity. Therefore, these results indicate that MoS_2 nanochains are excellent favorable gas sensing materials for the detection of ammonia at room temperature, which could stimulate greater innovation for future sensor technologies. Thus, the results of the present study may provide a new pathway to develop advanced nanocomposites for room-temperature gas-sensitive materials.

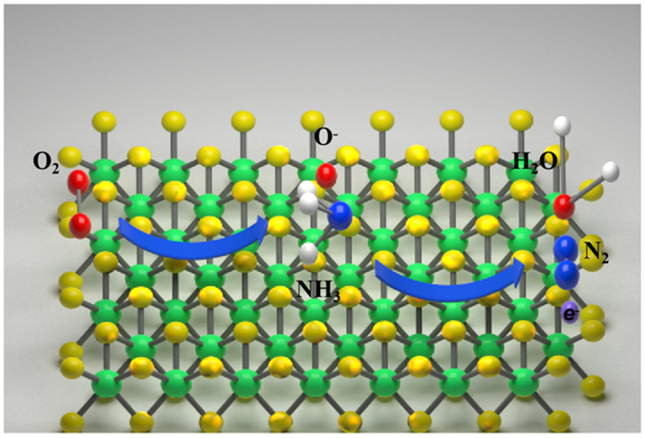

Figure 10. Process diagram of the MoS_2 nanochain gas sensing mechanism.

AUTHOR INFORMATION

Corresponding Author

Kai Zhuo − *MicroNano System research Center, Key Lab of Advanced Transducers and Intelligent Control System (Ministry of Education) & College of Information Engineering, Taiyuan University of Technology, Taiyuan 030024, China;* orcid.org/0000-0003-2966-9376; Email: zhuokai@tyut.edu.cn

Authors

Aoqun Jian − *MicroNano System research Center, Key Lab of Advanced Transducers and Intelligent Control System (Ministry of Education) & College of Information Engineering, Taiyuan University of Technology, Taiyuan 030024, China;* orcid.org/0000-0002-6532-7595

Junhe Wang − *MicroNano System research Center, Key Lab of Advanced Transducers and Intelligent Control System (Ministry of Education) & College of Information Engineering, Taiyuan University of Technology, Taiyuan 030024, China*

Hongying Lin − *MicroNano System research Center, Key Lab of Advanced Transducers and Intelligent Control System (Ministry of Education) & College of Information Engineering, Taiyuan University of Technology, Taiyuan 030024, China*

Shiqiang Xu − *MicroNano System research Center, Key Lab of Advanced Transducers and Intelligent Control System (Ministry of Education) & College of Information Engineering, Taiyuan University of Technology, Taiyuan 030024, China*

Dan Han − *MicroNano System research Center, Key Lab of Advanced Transducers and Intelligent Control System (Ministry of Education) & College of Information*

https://doi.org/10.1021/acsomega.1c06456
ACS Omega 2022, 7, 11664−11670

Engineering, Taiyuan University of Technology, Taiyuan 030024, China

Zhongyun Yuan − *MicroNano System research Center, Key Lab of Advanced Transducers and Intelligent Control System (Ministry of Education) & College of Information Engineering, Taiyuan University of Technology, Taiyuan 030024, China;* orcid.org/0000-0002-2429-2592

Complete contact information is available at: https://pubs.acs.org/10.1021/acsomega.1c06456

Author Contributions

†A.J. and J.W. are contributed equally to this study.

Notes

The authors declare no competing financial interest.

■ ACKNOWLEDGMENTS

The authors gratefully acknowledge the financial support by the National Natural Science Foundation of China (Nos. 62031022 and 51975400), Research Project Supported by Shanxi Scholarship Council of China (HGKY2019026), and International Cooperation of Science and Technology Projects in Shanxi Province (201903D421044).

■ REFERENCES

(1) Timmer, B.; Olthuis, W.; van den Berg, A. Ammonia sensors and their applications-a review. *Sens. Actuators, B* **2005**, *107*, 666−677.

(2) Mani, G. K.; Rayappan, J. B. B. A highly selective and wide range ammonia sensor—Nanostructured ZnO: Co thin film. *Mater. Sci. Eng., B* **2015**, *191*, 41−50.

(3) Kwak, D.; Lei, Y.; Maric, R. Ammonia gas sensors: A comprehensive review. *Talanta* **2019**, *204*, 713−730.

(4) Su, P.-G.; Yang, L.-Y. NH_3 gas sensor based on Pd/SnO_2/RGO ternary composite operated at room temperature. *Sens. Actuators, B* **2016**, *223*, 202−208.

(5) Qi, Q.; Wang, P. P.; Zhao, J.; Feng, L. L.; Zhou, L. J.; Xuan, R. F.; Liu, Y. P.; Li, G. D. SnO_2 nanoparticle-coated In_2O_3 nanofibers with improved AMMONIA sensing properties. *Sens. Actuators, B* **2014**, *194*, 440−446.

(6) Wang, L.; Lou, Z.; Zhang, R.; Zhou, T.; Deng, J.; Zhang, T. Hybrid Co_3O_4/SnO_2 Core-Shell Nanospheres as Real-Time Rapid-Response Sensors for Ammonia Gas. *ACS Appl. Mater. Interfaces* **2016**, *8*, 6539−6545.

(7) Korotcenkov, G. Metal oxides for solid-state gas sensors: What determines our choice? *Mater. Sci. Eng., B* **2007**, *139*, 1−23.

(8) Liu, N.; Paul, K.; Kim, J. H.; Ye, J. H.; Kim, S.; Lee, C. J. Large-Area Atomically Thin MoS_2 Nanosheets Prepared Using Electrochemical Exfoliation. *ACS Nano* **2014**, *8*, 6902−6910.

(9) Abun, A.; Huang, B. R.; Saravanan, A.; Kathiravan, D.; Hong, P. D. Effect of PMMA on the surface of exfoliated MoS_2 nanosheets and their highly enhanced ammonia gas sensing properties at room temperature. *J. Alloys Compd.* **2020**, *832*, No. 155005.

(10) Ko, D.; Jin, X.; Seong, K. D.; Yan, B.; Chai, H.; Kim, J. M.; Hwang, M.; Choi, J.; Zhang, W.; Piao, Y. Few-layered MoS_2 vertically aligned on 3D interconnected porous carbon nanosheets for hydrogen evolution. *Appl. Catal., B* **2019**, *248*, 357−365.

(11) Luo, Y.; Zhang, P.; Xiong, X.; Fu, H. Self-assembled MoS_2/C Nanoflowers with Expanded Interlayer Spacing as a High-Performance Anode for Sodium-Ion Batteries. *Chin. J. Chem. Eng.* **2021**, *39*, 240−246.

(12) Asaithambi, S.; Sakthivel, P.; Karuppaiah, M.; Balamurugan, K.; Yuvakkumar, R.; Thambidurai, M.; Ravi, G. Synthesis, and characterization of various transition metals doped SnO_2@MoS_2 composites for supercapacitor and photocatalytic applications. *J. Alloys Compd.* **2021**, *853*, No. 157060.

(13) Kumar, R.; Goel, N.; Kumar, M. UV-Activated MoS_2 Based Fast and Reversible NO_2 Sensor at Room Temperature. *ACS Sens.* **2017**, *2*, 1744−1752.

(14) Yu, H.; Xu, H.; Li, W.; Zhai, T.; Chen, Z.; Wang, J.; Cao, B. Enhanced triethylamine sensing properties by designing Au@SnO_2/ZnO nanosheets directly on alumina tubes. *Surf. Interfaces* **2018**, *10*, 85−92.

(15) Yao, Y.; Tolentino, L.; Yang, Z.; Song, X.; Zhang, W.; Chen, Y.; Wong, Cp. High-Concentration Aqueous Dispersions of MoS_2. *Adv. Funct. Mater.* **2013**, *23*, 3577−3583.

(16) Gatensby, R.; McEvoy, N.; Lee, K.; Hallam, T.; Berner, N. C.; Rezvani, E.; Winters, S.; O'Brien, M.; Duesberg, G. S. Controlled synthesis of transition metal dichalcogenide thin films for electronic applications. *Appl. Surf. Sci.* **2014**, *297*, 139−146.

(17) Chang, K.; Chen, W.; Ma, L.; Li, H.; Li, H.; Huang, F.; Xu, Z.; Zhang, Q.; Lee, J. Y. Graphene-like MoS_2/amorphous carbon composites with high capacity and excellent stability as anode materials for lithium-ion batteries. *J. Mater. Chem.* **2011**, *21*, 6251−6257.

(18) Park, M.; Park, Y. J.; Chen, X.; Park, Y. K.; Kim, M. S.; Ahn, J. H. MoS_2-Based Tactile Sensor for Electronic Skin Applications. *Adv. Mater.* **2016**, *28*, 2556−2562.

(19) Zhao, S.; Li, Z.; Wang, G.; Liao, J.; Lv, S.; Zhu, Z. Highly enhanced response of MoS_2/porous silicon nanowire heterojunctions to NO_2 at room temperature. *RSC Adv.* **2018**, *8*, 11070−11077.

(20) Cui, S.; Wen, Z.; Huang, X.; Chang, J.; Chen, J. Stabilizing MoS_2 Nanosheets through SnO_2 Nanocrystal Decoration for High-Performance Gas Sensing in Air. *Small* **2015**, *11*, 2305−2313.

(21) Bhimanapati, G. R.; Hankins, T.; Lei, Y.; Vila, R. A.; Fuller, I.; Terrones, M.; Robinson, J. A. Growth and Tunable Surface Wettability of Vertical MoS_2 Layers for Improved Hydrogen Evolution Reactions. *ACS Appl. Mater. Interfaces* **2016**, *8*, 22190−22195.

(22) Tan, H. M.; Hung, C. M.; Ngoc, T. M.; Nguyen, H.; Duc Hoa, N.; Duy, N. V.; Hieu, N. V. Novel Self-Heated Gas Sensors Using on-Chip Networked Nanowires with Ultralow Power Consumption. *ACS Appl. Mater. Interfaces* **2017**, *9*, 6153−6162.

(23) Yang, Z.; Zhang, D.; Chen, H. MOF-derived indium oxide hollow microtubes/MoS_2 nanoparticles for NO_2 gas sensing. *Sens. Actuators, B* **2019**, *300*, No. 127037.

(24) Yan, H.; Song, P.; Zhang, S.; Zhang, J.; Yang, Z.; Wang, Q. A low-temperature gas sensor based on Au-loaded MoS_2 hierarchical nanostructures for detecting ammonia. *Ceram. Int.* **2016**, *42*, 9327−9331.

(25) Singh, S.; Sharma, S. Ammonia sensing using MoS_2/WO_3 composite obtained via top-down approach. *Mater. Today: Proc.* **2021**, *43*, 137−140.

(26) Singh, S.; Kumar, S.; Sharma, S. Room-temperature high-performance ammonia sensor using MoS_2/SnO_2 nanocomposite. *Mater. Today: Proc.* **2020**, *28*, 52−55.

(27) Wang, W.; Zhen, Y.; Zhang, J.; Li, Y.; Zhong, H.; Jia, Z.; Xiong, Y.; Xue, Q.; Yan, Y.; Alharbi, N. S.; Hayat, T. SnO_2 nanoparticles-modified 3D-multilayer MoS_2 nanosheets for ammonia gas sensing at room temperature. *Sens. Actuators, B* **2020**, *321*, No. 128471.

(28) Wu, M.; He, M.; Hu, Q.; Wu, Q.; Sun, G.; Xie, L.; Zhang, Z.; Zhu, Z.; Zhou, A. Ti_3C_2 MXene-Based Sensors with High Selectivity for AMMONIA Detection at Room Temperature. *ACS Sens* **2019**, *4*, 2763−2770.

(29) Khuspe, G. D.; Navale, S. T.; Bandgar, D. K.; Sakhare, R. D.; Chougule, M. A.; Patil, V. B. SnO_2 nanoparticles-modified polyaniline films as highly selective, sensitive, reproducible, and stable ammonia sensors. *Electron. Mater. Lett.* **2014**, *10*, 191−197.

(30) Jiménez, I.; Centeno, M. A.; Scotti, R.; Morazzoni, F.; Arbiol, J.; Cornet, A.; Morante, J. R. AMMONIA interaction with chromium-doped WO_3 nanocrystalline powders for gas sensing applications. *J. Mater. Chem.* **2004**, *14*, 2412−2420.